AGU PUBLICATIONS

JGR

Journal of Geophysical Research: Oceans

RESEARCH ARTICLE

10.1002/2017JC013187

# Toward Understanding the Diverse Impacts of Air-Sea Interactions on MJO Simulations

**Joshua-Xiouhua Fu[1,2,3], Wanqiu Wang[4], Toshiaki Shinoda[5], Hong-Li Ren[3], and Xiaolong Jia[3]**

[1]IPRC, SOEST, University of Hawaii at Manoa, Honolulu, HI, USA, [2]Institute of Atmospheric Sciences, FuDan University, Shanghai, China, [3]National Climate Center, China Meteorological Administration, Beijing, China, [4]Climate Prediction Center, NOAA/NWS/NCEP, College Park, MD, USA, [5]Texas A&M University-Corpus Christi, Corpus Christi, TX, USA

**Key Points:**
- During DYNAMO period, the Oct-MJO and Nov-MJO events are sustained by atmospheric internal dynamics and ocean feedback
- The diverse effects of air-sea coupling on MJO simulations can be attributed to three causes
- They are diverse air-sea coupling in nature, diverse behaviors of cumulus schemes, and diverse SST anomalies

**Correspondence to:**
J.-X. Fu,
xfu@hawaii.edu

**Citation:**
Fu, J.-X., Wang, W., Shinoda, T., Ren, H.-L., & Jia, X. (2017). Toward understanding the diverse impacts of air-sea interactions on MJO simulations. *Journal of Geophysical Research: Oceans*, *122*, 8855–8875. https://doi.org/10.1002/2017JC013187

Received 13 JUN 2017
Accepted 4 OCT 2017
Accepted article online 10 OCT 2017
Published online 19 NOV 2017

**Abstract** The role of air-sea interactions on MJO simulations has long been recognized. However, the reasons for the variation of the impacts of air-sea coupling among different models are still elusive. In this study, we used NCEP GFS under different cumulus schemes and SST conditions to explore this issue. We focused on the Oct-MJO and Nov-MJO during the DYNAMO IOP. We show that the effects of SST-feedback on MJO simulations not only vary between these two MJO events, but are also very sensitive to the specifics of cumulus schemes and intraseasonal SST forcing. The Oct-MJO basically reinvigorates over Indian Ocean in association with the arrival of global circumnavigating mode. The Nov-MJO is largely reinvigorated by a robust intraseasonal SST anomaly over Indian Ocean. We found that SST-feedback is crucial for the existence of the Nov-MJO, but has little effect on the Oct-MJO. This finding raises the possibility that the occurrence of some MJO events may be rooted in air-sea interactions. These results suggest that the diverse impacts of air-sea coupling on MJO simulations can be attributed to at least the following three potential causes: (i) diverse responses of ocean to individual MJO events in nature; (ii) diverse behaviors of various cumulus parameterizations; and (iii) diverse intraseasonal SST anomalies in coupled models. Either a too weak internal MJO mode in atmospheric models or a too weak intraseasonal SST anomaly in coupled models would lead to the underestimation of the impacts of air-sea coupling on MJO simulations.

## 1. Introduction

The Madden-Julian Oscillation (MJO) manifests as an eastward-propagating atmospheric couplet between large-scale convective envelope and planetary-scale circulations along the equator (Madden & Julian, 1971, 1972). Although the primary body of the MJO is in the tropics, its impacts are felt globally due to teleconnections (e.g., Donald et al., 2006; Flatau & Kim, 2013; Higgins & Mo, 1997; Knutson & Weickmann, 1987; Lin et al., 2009; Zhang, 2013). Given that the MJO has strongest convection and low-level circulations in the Indo-western Pacific warm-pool, Madden and Julian (1972) speculated that "this oscillation is likely associated with some sort of a feedback mechanism as that of sea-surface temperatures (SST) and atmospheric circulation (Bjerknes, 1969) or evaporation and precipitation."

The First Global Atmospheric Research Program (GARP) Global Experiment (FGGE) campaign provided global daily atmospheric and SST data for the entire year of 1979 to document the modulations of the eastward-propagating global MJO mode on the regional, northward-propagating monsoon intraseasonal oscillation (Krishnamurti et al., 1985; Lorenc, 1984). Krishnamurti et al. (1988) used the FGGE data to document the earliest observed evidence of air-sea interactions on intraseasonal time scales: significant fluctuations of the SST and surface heat fluxes during 30–60 days over the Indo-Pacific warm-pool. This finding further substantiated the speculation of Madden and Julian (1972) and motivated Krishnamurti to propose that "a combination of atmospheric internal instabilities and external SST forcing on intraseasonal time scales may enhance the atmospheric responses toward an eventual satisfactory simulation of intraseasonal oscillation."

Using a 10 day mean SST over the tropical western Pacific collected by the Japan Meteorological Agency from 1979 to 1984 along with the twice daily outgoing longwave radiation (OLR) from NOAA, Kawamura (1988) first documented the coherent evolutions of intraseasonal SST and convection over the equatorial

western Pacific during boreal summer with positive (negative) SST anomaly leading (trailing) enhanced convection by about 10–20 days. Kawamura also found that positive SST anomaly collocates with suppressed convection in the western Pacific along with active convection in the Indian Ocean and Maritime Continent. When the active convection moves into western Pacific, negative SST anomaly begins to develop. This scenario motivated Kawamura to suggest that "an air-sea feedback system appears to be rather significant for the 30–60 day oscillation," but he also noticed that "the air-sea coupling on the 30–60 day time scale was much weaker over the tropical western Pacific in 1981 than that in 1979."

Coherent air-sea interactions were further documented for two boreal-winter MJO events in late 1992 and early 1993 over the equatorial western Pacific during the Tropical Ocean Global Atmosphere Coupled Ocean Atmosphere Response Experiment (TOGA COARE) (Anderson et al., 1996; Shinoda et al., 1998). Following these observational studies, a few theoretical air-sea coupled models (e.g., Hirst & Lau, 1990; Lau & Shen, 1988; Li & Liao, 1996; Liu & Wang, 2013; Sobel & Gildor, 2003; Wang & Xie, 1998) were developed to assess the impacts of air-sea coupling on intraseasonal oscillations. All these coupled models are capable of producing sustained MJO-like oscillations. In these models, the SST anomaly feedbacks to the atmosphere through changing surface evaporation (Hirst & Lau, 1990; Lau & Shen, 1988; Liu & Wang, 2013; Sobel & Gildor, 2003) and/or diabatic heating (Liu & Wang, 2013; Wang & Xie, 1998).

Apart from these theoretical models, a hierarchy of air-sea coupled models with different atmospheric and oceanic components of varying complexities have been developed to assess the impacts of air-sea coupling on MJO simulations (e.g., Benedict & Randall, 2011; Crueger et al., 2013; Flatau et al., 1997; Fu & Wang, 2004; Grabowski, 2006; Green et al., 2017; Hendon, 2000; Inness et al., 2003; Liess et al., 2004; Kemball-Cook et al., 2002; Klingaman & Woolnough, 2014; Marshall et al., 2008; Sperber et al., 2005; Waliser et al., 1999; Watterson & Syktus, 2007). The atmospheric components range from a simple general circulation model (GCM, Flatau et al., 1997) to sophisticated conventional GCMs (e.g., Waliser et al., 1999) and superparameterized GCMs (e.g., Benedict & Randall, 2011; Grabowski, 2006). The ocean components span from a simple parameterization of SST as a function of surface winds (Flatau et al., 1997), slab mixed-layer (e.g., Benedict & Randall, 2011; Marshall et al., 2008; Waliser et al., 1999), 1-D mixed-layer (e.g., Klingaman & Woolnough, 2014), 2-1/2 layer upper ocean model (Fu & Wang, 2004; Kemball-Cook et al., 2002), to complex ocean GCMs (e.g., Crueger et al., 2013; Inness et al., 2003). Most of these modeling studies showed that interactive air-sea coupling improves MJO simulations in terms of intensity, coherence, and propagation. At the same time, some modeling studies show negligible or negative impacts of air-sea coupling on MJO simulations (e.g., Hendon, 2000; Liess et al., 2004; Miura et al., 2007; Newman et al., 2009). These diverse modeling results cast doubts on the degree of ocean coupling involved in MJO dynamics and call for better understanding of the diverse impacts of air-sea coupling on MJO simulations. The root causes of these diverse impacts are still elusive, although some previous studies have touched this issue.

Hendon (2000), Kemball-Cook et al. (2002), and Inness et al. (2003) suggested that ocean feedback on MJO simulations largely depends on the mean states. Zhang and Anderson (2003) attributed the diverse impacts of air-sea coupling to different MJO structures in the observations and models. Hendon (2000) found that the misrepresentation of westerly mean wind over the equatorial Indian and western Pacific Oceans in their coupled model results in the cancelation between intraseasonal solar radiation and surface evaporation perturbations, thus leading to negligible SST response and insignificant ocean feedback on model MJO. A substantial cold bias in an early version of the University of Hawaii (UH) hybrid coupled model (Kemball-Cook et al., 2002) is found to significantly degrade the simulations of monsoon mean flows and associated vertical shear and northward-propagating intraseasonal oscillation. In their fully coupled GCM, Inness et al. (2003) revealed that the lack of westerly mean wind over the equatorial western Pacific due to cold bias stalls the model MJO within the Indian basin. With flux correction, the warm-up of western Pacific allows the eastward extension of westerly mean wind, which leads the model MJO to propagate over the Maritime Continent and enter the western Pacific.

Zhang and Anderson (2003) divided the MJOs in the observations and models into four types (Type-I, Type-II, Type-III, and Type-IV) based on the phase relationship between convection and surface variables. For Type-I, weak easterly (strong westerly) precedes (lags) the peak precipitation (e.g., Kemball-Cook et al., 2002; Madden & Julian, 1972). For Type-II, weak easterly (strong westerly) precedes (collocates with) the peak precipitation (e.g., Inness et al., 2003). For Type-III, strong easterly (weak westerly) precedes (lags) the peak precipitation (e.g., Emanuel, 1987; Neelin et al., 1987). And for Type-IV, strong westerly (weak easterly)

lags (collocates with) the peak precipitation (e.g., Maloney & Hartmann, 2001; Wang & Li, 1994). Forcing a 1-d mixed-layer ocean model with the surface fluxes in association with the above four MJO types, they showed that the SST responses to the MJO are very sensitive to the structures of MJO surface variables. The resultant SST anomaly is largest for Type-II due to the coincidence of surface latent heat flux, solar radiation, and possibly entrainment and smallest for Type-IV because the heating and cooling by surface latent heat flux and solar radiation flux almost cancel each other. In addition, larger amplitude, longer period, slower propagation speed, and longer wavelength of the MJO will also lead to larger SST perturbations.

Fu et al. (2015) focused on the MJO events observed during the DYNAMO/Cooperative Indian Ocean Experiment on Intraseasonal Variability in Year 2011 (CINDY) period (October 2011 to March 2012; Yoneyama et al., 2013) and suggested that in the real world, the importance of ocean feedback on different MJO events might also be very different. Specifically, we found that the Oct-MJO during this period can be well reproduced without involving any intraseasonal SST-feedback, while the Nov-MJO cannot if intraseasonal SST-feedback is not well represented (e.g., S. G. Wang et al. 2015; W. Q. Wang et al., 2015). We further show that the initialized atmosphere-only model, which is driven by daily SST from the coupled run, reaches almost the same skill as the interactive atmosphere-ocean coupled runs. This result suggests that initialized atmosphere-only runs (also known as the Transpose-AMIP approach; Phillips et al., 2004) are an efficient way to capture the impacts of air-sea coupling and investigate the processes through which the SST feeds back to the MJO (e.g., de Boisseson et al., 2012; Fu et al., 2008; Pegion & Kirtman, 2008; W. Q. Wang et al. 2015). The origin of the positive SST anomaly preceding the Nov-MJO active phase has also been investigated by Moum et al. (2014), Chi et al. (2014), and de Szoeke et al. (2015). With detailed oceanic mixed-layer heat budget analysis, Chi et al. (2014) found that both surface heat fluxes and oceanic processes contribute to the positive SST anomaly with the former contributing slightly larger than the latter.

Given that various cumulus parameterizations have been used in present-day atmospheric models and the resultant intraseasonal SST perturbations vary widely among their coupled versions, we used a series of hindcasts carried out with the National Centers for Environmental Prediction (NCEP) global forecast system (GFS) under different cumulus schemes and different SST conditions (W. Q. Wang et al. 2015) in this study. The resultant MJO simulations under different combinations of cumulus schemes and SST conditions among these experiments will shed light on the possible causes of diverse impacts of air-sea coupling in present-day models. The major questions that will be addressed in this study include: (1) How do cumulus parameterizations impact MJO simulations under different SST conditions? (2) How does SST-feedback impact MJO simulations under different cumulus parameterizations? (3) Why are the impacts of air-sea coupling so different on the Oct-MJO and Nov-MJO?

The rest of this paper is structured as follows. In section 2, the model is described and the details of sensitivity experiments are given. Section 3 assesses the impacts of air-sea coupling on MJO simulations under different cumulus parameterizations and intraseasonal SST perturbations. As an extension of our previous studies (Fu et al., 2013, 2015; W. Q. Wang et al. 2015), section 4 focuses on the case study of the Oct-MJO and Nov-MJO during the DYNAMO period. Finally, discussions and concluding remarks are given in section 5.

## 2. Model and Sensitivity Experiments

In order to better understand and improve the air-sea interactions in the NCEP Climate Forecast System (CFS), a series of hindcasts with the atmospheric component (the GFS) under different cumulus parameterizations and intraseasonal SST perturbations were carried out (W. Q. Wang et al. 2015). The NCEP GFS used in this study has a horizontal resolution of T126 with 64 vertical levels. The atmospheric model physics are the same as that of the CFSv2 (Saha et al., 2014). In addition to the Simplified Arakawa-Schubert (SAS) scheme used for the CFSv2, the GFS has other two variants of the AS convection schemes: the Relaxed Arakawa-Schubert (RAS) and Simplified Arakawa-Schubert version 2 (SAS2). A brief summary of these three convection schemes is given here for convenience. More details can be found in W. Q. Wang et al. (2015) and references therein.

The SAS scheme used in the CFSv2 is based on Arakawa and Schubert (1974) and modified by Pan and Wu (1995). The RAS developed by Moorthi and Suarez (1992, 1999) simplifies the treatments of normalized mass flux and relaxes the required "quasi equilibrium" in the original AS scheme. The SAS2 (Han & Pan, 2011) is the scheme used in current operational GFS, which includes modifications to the SAS by increasing

the cloud-base mass flux and enhancing the sensitivity of entrainment and detrainment to environmental moisture (Bechtold et al., 2008).

In total, nine sets of initialized hindcasts with the GFS were carried out during the DYNAMO IOP (1 October 2011–15 January 2012) with the above three cumulus schemes under three SST settings. The initial conditions of all experiments are taken from NCEP Climate Forecast System Reanalysis (CFSR; Saha et al., 2010). The NCDC daily SST (Reynolds & Smith, 1994), TMI daily SST (Wentz et al., 2000), and the long-term climatology of the NCDC SST (referred as NCDC, TMI, and CLIM hereafter) are used as sea surface conditions for the hindcasts. Only the first two SST data sets contain intraseasonal signals. Although the interactive coupled models should be the perfect platform to study the impacts of air-sea coupling, the results obtained from those models are often contaminated by unavoidable mean-state biases (e.g., DeMott et al., 2015). On the other hand, the initialized atmosphere-only approach is a proven alternative as demonstrated in previous studies (e.g., de Boisseson et al., 2012; Fu et al., 2008, 2013, 2015; Pegion & Kirtman, 2008; W. Q. Wang et al. 2015). This approach is effective at avoiding the mean-state drift problems that plague the coupled models. Because the intraseasonal SST perturbations in the NCDC are much smaller than that in the TMI (e.g., Harrison & Vecchi, 2001; Senguta et al., 2001), it is expected that the MJO differences among the runs forced by the CLIM, NCDC, and TMI SSTs will reveal the impacts of different amplitudes of SST perturbations on MJO simulations. The MJO differences among the three cumulus parameterizations under a given SST condition will show the impacts of cumulus schemes on the SST-feedbacks.

Each of the nine experiments consists of 30 day hindcasts initialized four times (0000, 0600, 1200, and 1800 UTC) each day during the DYNAMO IOP. In this study, we only use the hindcasts initialized in October and November (61 days in total). The same initial conditions from the CFSR were used for the nine experiments. The procedure used to derive the intraseasonal anomalies from the hindcasts is similar as that used in W. Q. Wang et al. (2015). First, the four times per day hindcasts are averaged to obtain a daily ensemble mean. Next, a second-order polynomial fit is used to extract the seasonal mean states at each lead time. Raw anomalies are derived as the differences between the total and seasonal means. Finally, intraseasonal anomalies are obtained by removing synoptic variability from the raw anomalies with 5 day running mean. The observations used in this study include daily NOAA OLR, TRMM precipitation, and TMI SST. The same procedure used for the hindcasts was used to obtain the observed intraseasonal anomalies.

## 3. Impacts of Different Cumulus Schemes and SST Conditions

### 3.1. Evaluations of Intraseasonal Convective Anomalies

In order to illustrate the respective impacts of three cumulus schemes and three SST settings, Figure 1 shows the longitude-time evolutions of simulated OLR anomalies at lead time of day 15 over the Indo-western Pacific sector from the nine hindcasts. The corresponding observations are also given. As expected from Fu et al. (2015), the Oct-MJO is much better simulated than the Nov-MJO when there is no intraseasonal SST forcing, no matter which cumulus scheme was used (Figures 1a–1c). Relatively speaking, the simulations with the RAS and SAS are better than that with the SAS2, which highlights the severe problems of operational GFS and explains its very limited MJO forecasting skill (Fu et al., 2013; Hamill & Kiladis, 2014; Matsueda & Endo, 2011). When forced with NCDC SST (Figures 1d–1f), the improvements from SST-feedback are very small due to weak intraseasonal SST anomaly. When daily TMI SST is used (Figures 1g–1i), the SST-feedback results in very strong responses with the RAS and SAS (Figures 1g and 1h), in particular for the Nov-MJO, but still very weak with the SAS2 (Figure 1i). The resultant MJO with the RAS and SAS schemes is in much better agreement with the corresponding observations than that with the SAS2 scheme.

Figure 2 gives the simulated OLR anomalies with three cumulus schemes under climatological SST at different lead times. Because there is no intraseasonal SST forcing during the hindcast period, this result can be viewed as the effect of atmospheric internal dynamics under different cumulus schemes. The GFS with the RAS and SAS schemes is able to capture the life cycle of the Oct-MJO with some realism even at day 15 (Figures 2a, 2b, 2e, 2f, 2i, and 2j), although the simulations have an apparent phase delay compared to the observations (Figures 2d, 2h, and 2l). This result suggests that the Oct-MJO in the model develops slower than that in the observations. The simulations with the SAS2 perform poorly after day 10 (Figures 2c and 2g).

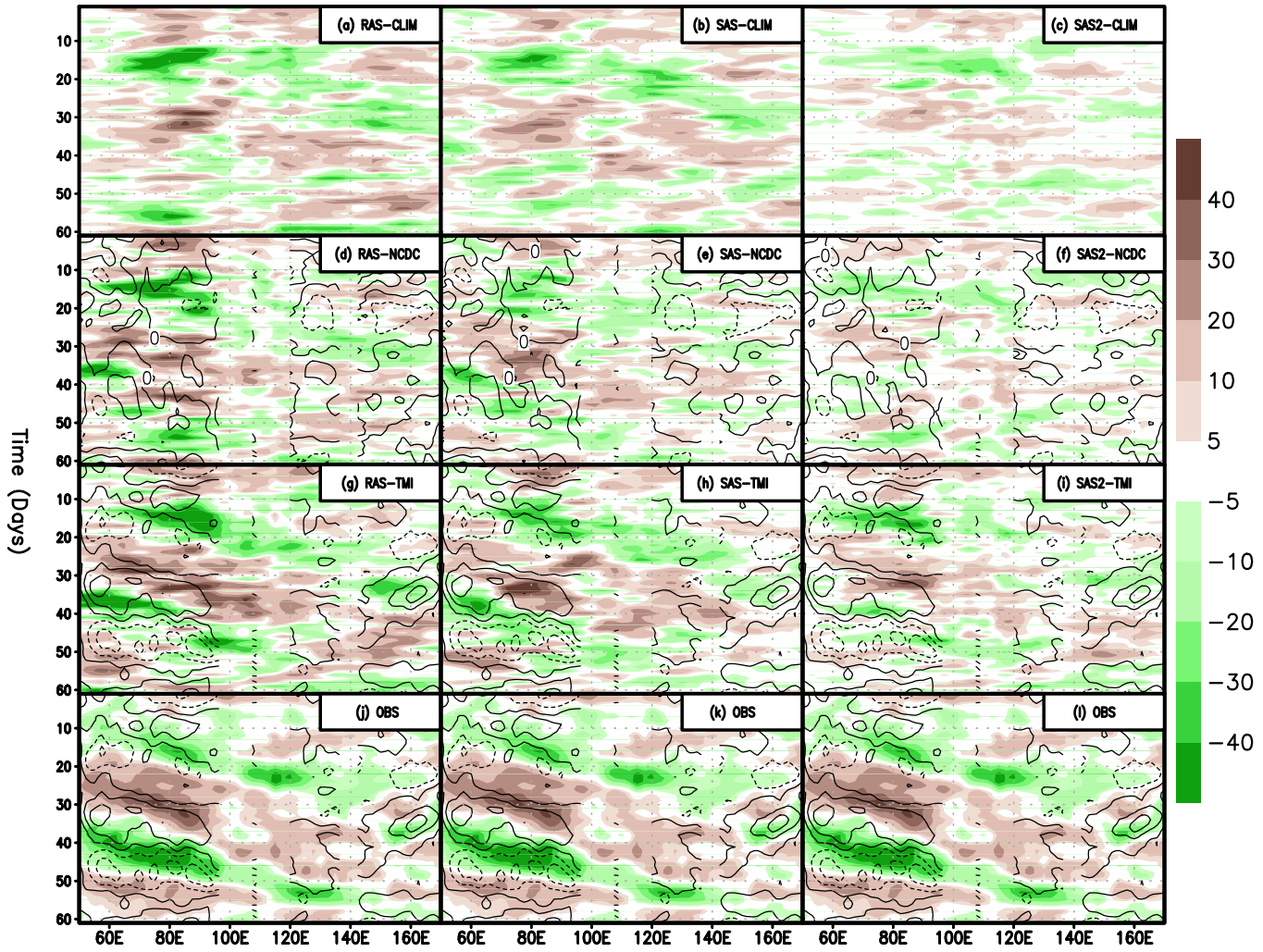


**Figure 1.** Longitude-time evolutions of simulated OLR (shading, W $m^{-2}$) and SST anomalies (contours, CI: 0.2°C) averaged between 10°S and 10°N at lead time of day 15 for the (a, d, g) RAS, (b, e, h) SAS, and (c, f, i) SAS2 cumulus schemes, respectively, forced by climatological SST (CLIM), NCDC SST, and TMI SST along with the observations (j, k, l). The ordinate starts from 15 October 2011.

Similar as what was found in Fu et al. (2015) with UH-hybrid coupled model, none of the simulations in this case are able to reproduce the Nov-MJO after a10 day lead.

Figure 3 shows the simulated OLR anomalies under three cumulus schemes when more realistic intraseasonal SST forcing (i.e., TMI SST) is exerted during the hindcast period. This result can be viewed as the combined effects of atmospheric internal dynamics and external SST forcing. In this case, the resultant Oct-MJO looks much more coherent compared to that without intraseasonal SST forcing (Figure 2). The simulations of the Nov-MJO improved across all three cumulus schemes. Remarkable improvements occur for the RAS and SAS where the results agree well with the observations even beyond 20 days (Figures 3a, 3b, 3e, 3f, 3i, 3j, 3m, and 3n). The results with the SAS2 (Figures 3c, 3g, 3k, 3o, and 3s) are still much weaker than the observations after about 10 days.

To further examine the impacts of intraseasonal SST forcing under three cumulus schemes, Figure 4 shows the simulated OLR differences between that forced by daily TMI SST and climatological SST. The significant impact of the intraseasonally varying SST anomaly on the model MJO can be seen as early as day 3 with the RAS and SAS2 (Figures 4a and 4c). The SAS has slowest response to intraseasonally varying SST forcing (Figures 4b and 4e). As the lead time increases, the response to intraseasonal SST anomaly with the SAS2 does not show any significant amplification, while the simulations with the RAS and SAS show very strong responses to intraseasonal SST anomaly even beyond 30 days, especially for the RAS scheme.

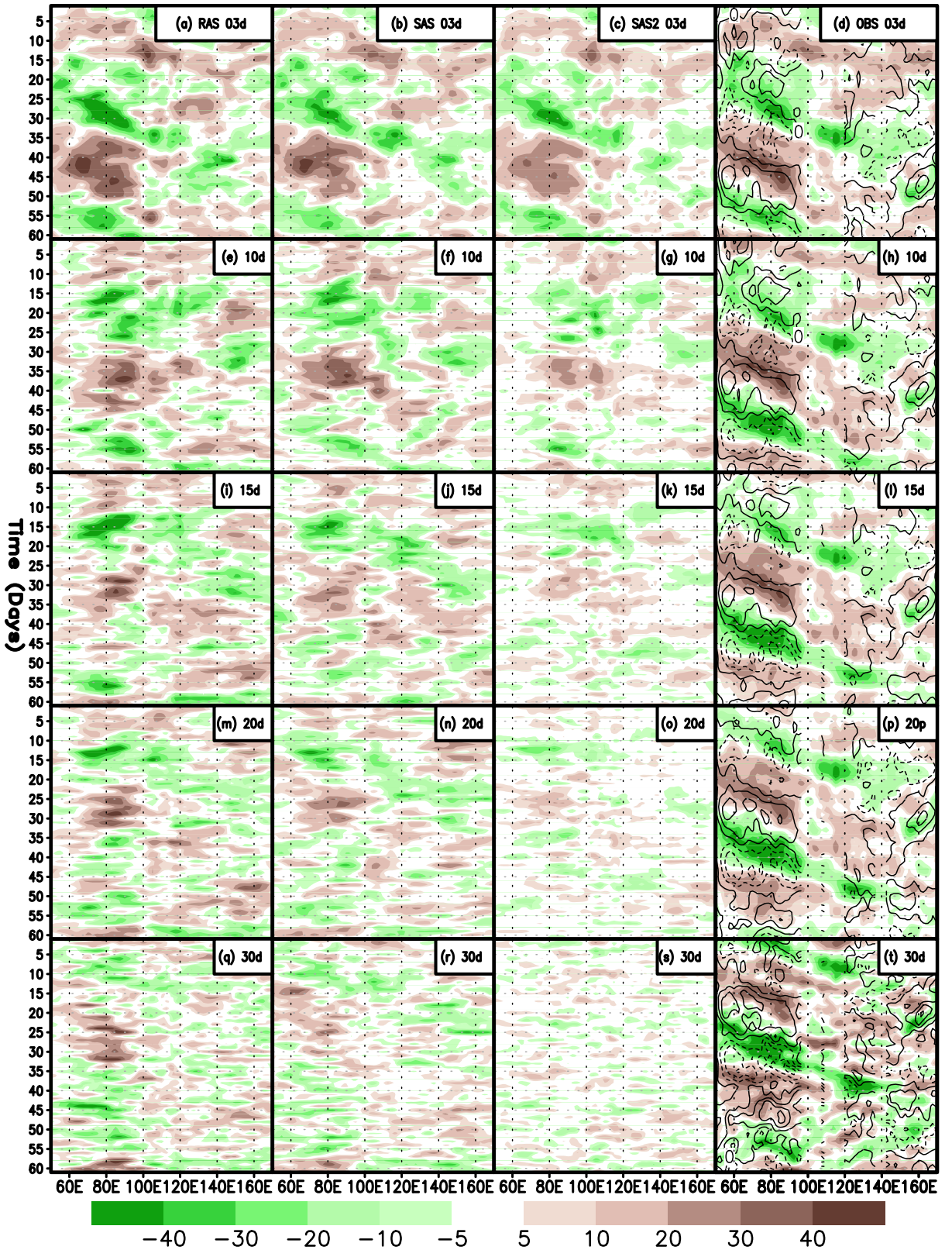


**Figure 2.** Longitude-time evolutions of OLR anomalies (shading, W $m^{-2}$) averaged between 10°S and 10°N for the (a, e, i, m, q) RAS, (b, f, j, n, r) SAS, and (c, g, k, o, s) SAS2 cumulus schemes forced by climatological SST and corresponding observations (d, h, l, p, t) at lead times of days 3, 10, 15, 20, and 30 with the ordinate starting, respectively, from 3 October, 10 October, 15 October, 20 October, and 30 October 2011.

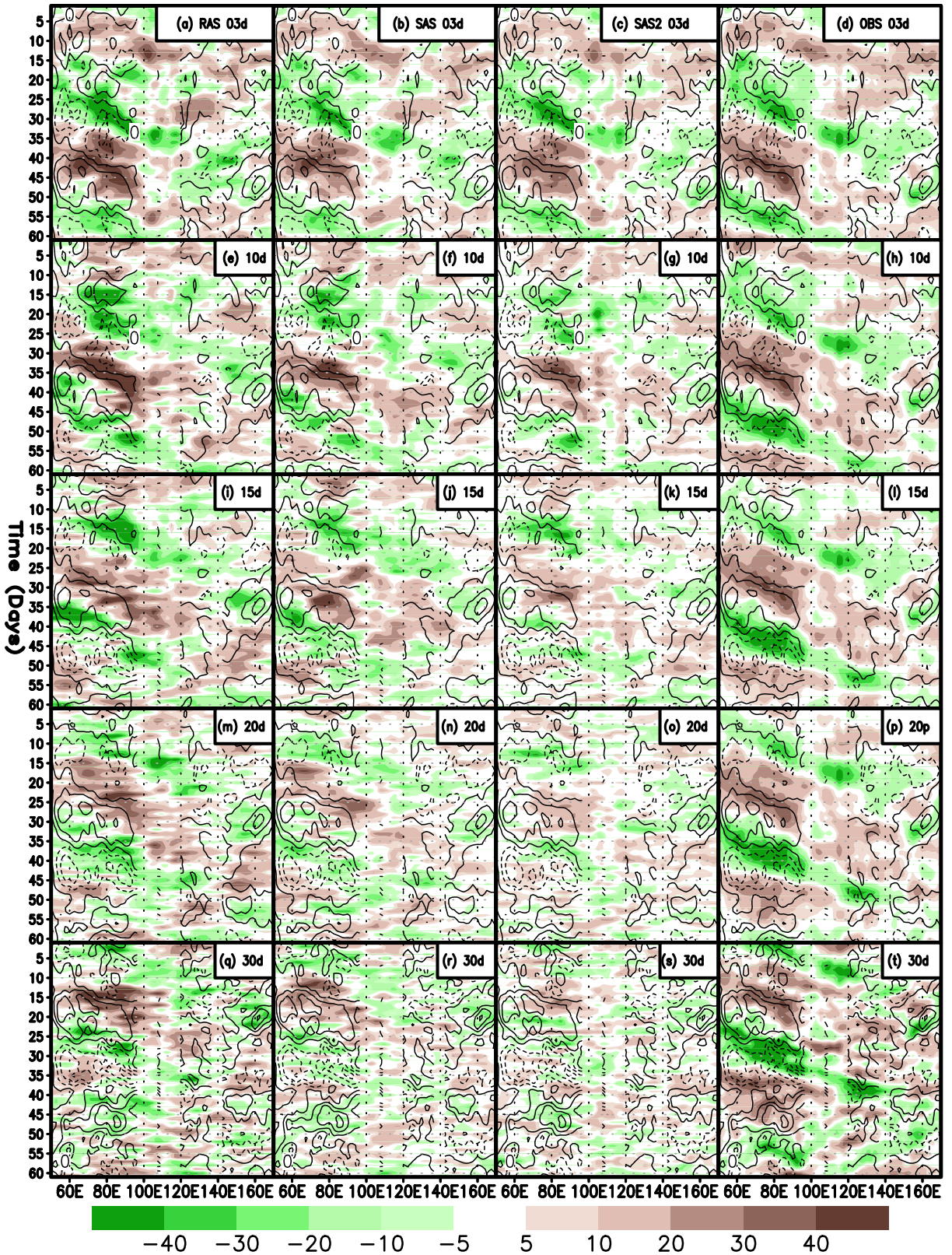


**Figure 3.** Longitude-time evolutions of OLR (shading, W $m^{-2}$) and SST anomalies (contours, CI: 0.2°C) averaged between 10°S and 10°N for the (a, e, i, m, q) RAS, (b, f, j, n, r) SAS, and (c, g, k, o, s) SAS2 cumulus schemes forced by TMI SST and corresponding observations (d, h, l, p, t) at lead times of days 3, 10, 15, 20, and 30 with the ordinate starting, respectively, from 3 October, 10 October, 15 October, 20 October, and 30 October 2011.

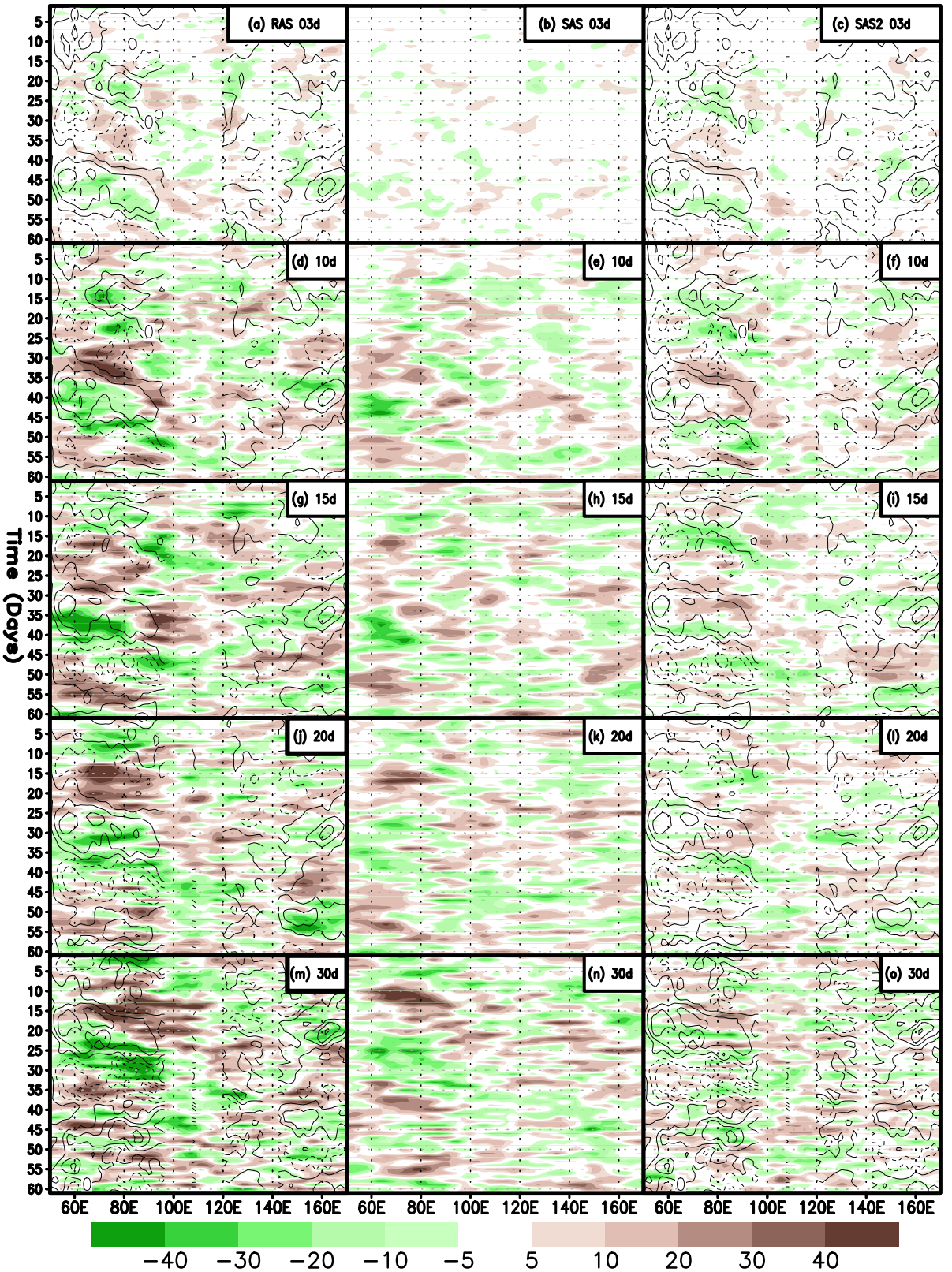


**Figure 4.** Differences of OLR (shading, W $m^{-2}$) and SST anomalies (contours, CI: 0.2°C) averaged over 10°S and 10°N between the simulations forced by TMI and climatological SST for the (a, d, g, j, m) RAS, (b, e, h, k, n) SAS, and (c, f, i, l, o) SAS2 cumulus schemes at lead times of days 3, 10, 15, 20, and 30 with the ordinate starting, respectively, from 3 October, 10 October, 15 October, 20 October, and 30 October 2011.

The above results suggest that if the MJO in the simulation forced with climatological SST is too weak (e.g., the SAS2), the SST-feedback will also be weak (e.g., Watterson & Syktus, 2007). If an atmospheric model has a strong internal MJO mode (e.g., the RAS), the SST-feedback is likely to also be robust. If an air-sea coupled model produces a weak SST anomaly (e.g., the case with the NCDC SST, coupled model used by Hendon (2000), and models producing type-IV MJO depicted in Zhang and Anderson (2003)), the resultant effects of air-sea coupling on MJO simulations will be underestimated.

### 3.2. Quantitative Measure of the Impacts

In this section, the impacts of SST-feedbacks on MJO simulations in the nine experiments are quantified with Anomaly Correlation Coefficient (ACC), Root-Mean-Square-Error (RMSE), and intensity that are defined as the standard deviations of intraseasonal OLR anomalies in the observations and individual experiments. The ACC is defined as the pattern correlation between simulated longitude-time OLR anomaly field and observed longitude-time OLR anomaly field at lead times of 1–30 day (e.g., the ACCs under climatological SST with the RAS, SAS, and SAS2 schemes at lead time of day 3 are calculated between Figures 2d and 2a–2c). The RMSE is defined as the root-mean-square of the difference between simulated longitude-time OLR anomaly field and observed longitude-time OLR anomaly field at lead times of 1–30 day (e.g., the RMSEs under climatological SST with the RAS, SAS, and SAS2 schemes at lead time of day 3 are calculated between Figures 2d and Figures 2a–2c).

Figures 5 and 6 show the MJO skills measured with the ACC, RMSE, and intensity of nine hindcasts and the differences between forcing with the NCDC/TMI SSTs and with climatological SST under three cumulus schemes. When forced with climatological SST, the MJO skills measured by the ACC are actually very similar among the three cumulus schemes with the skills of the RAS and SAS2 slightly lower than that of the SAS (Figure 5a). The MJO intensity is strongest for the RAS, weakest for the SAS2, with the SAS in the middle (Figure 6a). When measured with the RMSE (Figure 5c), the RAS has the largest bias, likely due to the phase difference between the simulations and observations (Figure 2). The SAS2 has the smallest RMSE because the amplitude of the simulated anomalies is weak and the RMSE is largely contributed by the observed anomalies. When forced with the NCDC SST, the overall impacts of SST-feedback on MJO simulations under all three cumulus schemes are marginal and insignificant.

When forced with the TMI SST (Figures 5 and 6), all three cumulus schemes indicate robust skill gains compared to that forced by climatological SST with the gain of the RAS (SAS2) being the largest (smallest). The impacts of TMI SST on the ACCs almost linearly increase from zero to around 0.5 during the 30 day integration for the RAS and SAS (Figure 5b). However, the gain for the SAS2 increases from zero to a maximum of 0.2 around day 15, drops to zero at day 20, and bounces up again to about 0.2 at day 28. The TMI SST reduces the RMSEs for the RAS and SAS considerably (Figure 5d), but only has marginal and mixed impact for the SAS2. The TMI SST also systematically increases the MJO intensity for all three cumulus schemes (Figure 6b). The resultant MJO intensity gets closer to the observations for the SAS and RAS, but is still too weak for the SAS2 (Figure 6a).

If we define the time when the ACC drops to 0.5 as the prediction skill, the MJO skills are around 7 days for all three cumulus schemes (Figure 5a) forced with climatological and NCDC SSTs. The TMI SST increases the skill of the SAS2 slightly to 9 days, the SAS to 15 days, and the RAS to 12–22 days (Figure 5a). The large skill range for the RAS is because the skill line levels around 0.5 over the period. If we take the ACC differences between that forced with TMI SST and that with climatological SST (Figure 5b) as a measure of SST-feedback strength to the MJO (or air-sea coupling strength), the feedback with the RAS is the strongest. Considering that the simulations with the RAS have the best agreement with the observations (Figure 3), it is reasonable to assume that the simulations with the RAS might reflect the SST-feedback in the real world. Along this line, the SST-feedbacks with the SAS2 and SAS were underestimated, in particular with the SAS2 (Figure 5b).

If we take the results forced with climatological SST as the effect of atmospheric internal dynamics on sustaining MJO mode, the capability of atmospheric internal dynamics represented by three cumulus schemes does not differentiate much in terms of the ACC, which drops below 0.3 after about 12 days (Figure 5a). The feedback from the TMI SST with the RAS starts to contribute more than 0.3 to the total skill after about 12 days (Figure 5b). This result suggests that beyond $\sim$12 days, the skill gain from SST-feedback alone exceeds the skill originating from the initial conditions and sustained by the atmospheric internal dynamics.

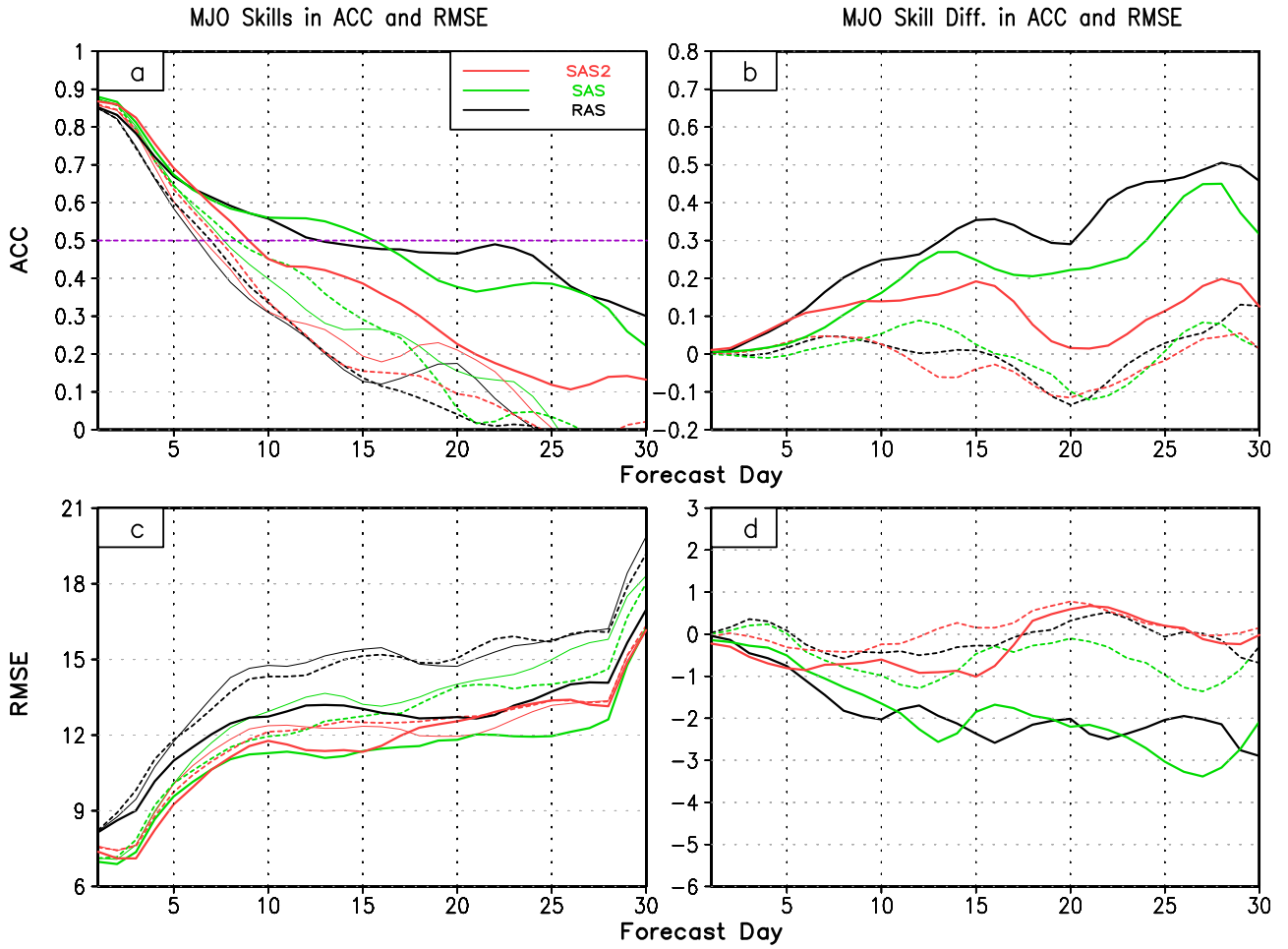


**Figure 5.** MJO skills measured with (a) anomalous correlation coefficient (ACC) and (c) root-mean-square-error (RMSE) as a function of lead times with the RAS, SAS, and SAS2 cumulus schemes forced by climatological SST (thin solid lines), NCDC SST (dashed lines), and TMI SST (thick solid lines) and skill differences (b, d) forced by NCDC SST anomaly (dashed lines) and TMI SST anomaly (thick solid lines).

It is intriguing to note that when forced with climatological SST, the skills measured with the ACC are actually very similar among the runs with the RAS, SAS, and SAS2 schemes, but significantly different when forced with TMI SST. This result might suggest that, in atmosphere-only free runs forced by any SSTs or in the initialized hindcast/forecasting runs driven by monthly SST or any other SSTs without realistic intraseasonal anomaly, the ACC alone is not necessarily the best measure of MJO quality or the adequacy of a specific cumulus parameterization in representing the MJO. On the other hand, it is the response to the realistic intraseasonal SST anomaly that helps reveal which cumulus parameterization is the best for realistic simulation and prediction of the MJO.

The above analyses showed that the impacts of SST-feedbacks on MJO simulations strongly depend on the cumulus schemes. At the same time, the quality of a specific cumulus scheme to represent the MJO varies with underlying sea surface conditions too (Figure 7). Under climatological and NCDC SSTs, the RAS and SAS2 have similar ACCs (Figure 7a), but the RAS has consistently larger RMSE and intensity than the SAS2 (Figures 7c and 7d); the SAS has slightly higher ACC than the SAS2 (Figure 7a), but also consistently larger RMSE and intensity than the SAS2 (Figures 7c and 7d). Under the TMI SST, the RAS and SAS have much higher ACCs and intensity than the SAS2 (Figures 7a and 7b) along with similar or reduced RMSEs (Figure 7c). This result indicates that under either climatological and NCDC SSTs, the MJO skills measured by the ACC, RMSE, and intensity show mixed quality among the three cumulus schemes. Only when forced with TMI SST, the MJO skills measured with the ACC, RMSE, and intensity consistently show that the RAS and SAS are better schemes than the SAS2 in representing the MJO. It is worth mentioning that, relative to the ACC

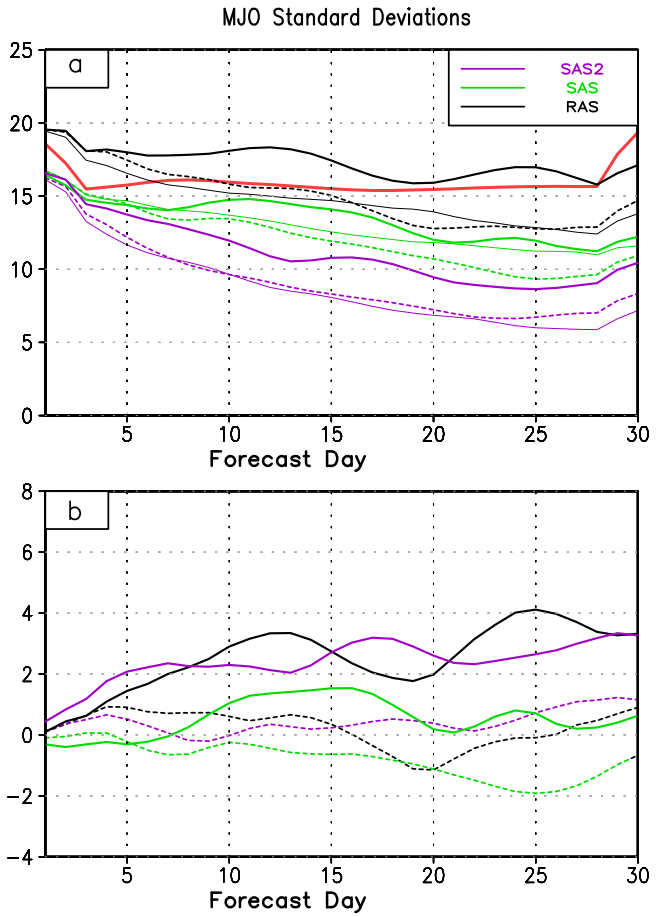


**Figure 6.** MJO intensities (a) measured with the standard deviations of intraseasonal OLR anomalies as a function of lead times with the RAS, SAS, and SAS2 cumulus schemes forced by climatological SST (thin solid lines), NCDC SST (dashed lines), TMI SST (thick solid lines), and from the observations (thick red line) along with the intensity differences (b) forced by NCDC SST anomaly (dashed lines) and TMI SST anomaly (thick solid lines).

and RMSE, the intensity of the RAS is always stronger than that of the SAS and SAS2 no matter what the SST forcing (Figures 6a and 7b). This suggests that the MJO intensity is likely a better index than the ACC and RMSE as an indicator of model capability in representing the MJO when no realistic intraseasonal SST forcing is applied (e.g., climatological and NCDC SSTs).

## 4. Different Impacts of Air-Sea Coupling on Oct-MJO and Nov-MJO

In the above section, we show that the simulations of the Oct-MJO and Nov-MJO with the RAS scheme forced by TMI SST agrees well with the observations (Figure 3) and the associated SST-feedback can be viewed as a good representative of what happens in the real world (Figures 5 and 6), whereas the feedback with the SAS2 is considerably underestimated. In this section, we closely examine the hindcasts of the Oct-MJO and Nov-MJO, respectively, with the RAS and SAS2 schemes forced by TMI SST. The goal is to provide a better understanding of why the impacts of air-sea coupling on these two MJOs are so different (Fu et al., 2015).

Figures 8 and 9 show the hindcasts of Oct-MJO and Nov-MJO in total and anomalous OLR fields with the RAS and SAS2 forced by climatological SST and TMI SST along with observations, respectively, initialized on 13 October and 7 November 2011. For the Oct-MJO, the hindcasts with the RAS are able to capture its onset and eastward propagation with and without intraseasonal SST forcing (Figures 8c, 8d, 8e, and 8f). The mean states with the SAS2 (Figures 8g and 8i), however, are much drier than that with the RAS and the intraseasonal variability is weak (Figures 8h and 8j). Although weak, the SAS2 also produces an active phase over the Indian Ocean during the passage of the observed Oct-MJO. With the known strength and weakness of these two cumulus schemes from previous section, this result suggests that both the onset and eastward propagation of the Oct-MJO are largely controlled by atmospheric internal dynamics, while SST-feedback makes the simulation more coherent (Figures 8f and 8j). The scenario for the Nov-MJO is considerably different (Figure 9). The hindcasts without intraseasonal SST anomaly almost totally miss this event no matter which cumulus scheme is used (Figures 9d and 9h). On the other hand, the hindcasts with intraseasonal SST forcing capture this event well using the RAS (Figure 9f). The SAS2 also captures this event with weak intensity (Figure 9j), although the mean states with the SAS2 are still too dry (Figures 9g and 9i).

It is worth mentioning that, for the Oct-MJO, the positive SST anomaly is almost in phase with the convection in both the observations and hindcasts (Figures 8b, 8f, and 8j), while the positive SST anomaly leads the convection by a few days for the Nov-MJO (Figures 9b, 9f, and 9j). This result suggests that the preconditioning of the Oct-MJO has little to do with the associated positive SST anomaly. On the other hand, the preceding positive SST anomaly may play an essential role to precondition the onset of the Nov-MJO. Note that, at least for these two hindcast periods, the dry (wet) mean states coexist with weak (strong) MJO signals (Figures 8c, 8e, 8g, 8i and Figures 9c, 9e, 9g, 9i). It is difficult to attribute any causal relationship between the mean and MJO magnitude from these results. As suggested by Hoyos and Webster (2007), it is likely that they positively interact with each other.

In order to further understand what drive the Oct-MJO and Nov-MJO, Figures 10 and 11 compare the simulated spatiotemporal evolutions of OLR, 200 hPa velocity potential, and SST anomalies in association with the Oct-MJO and Nov-MJO for the RAS scheme forced by climatological SST and TMI SST. For the Oct-MJO (Figure 10), the organized convection first appears in the southwestern Indian Ocean in association with the

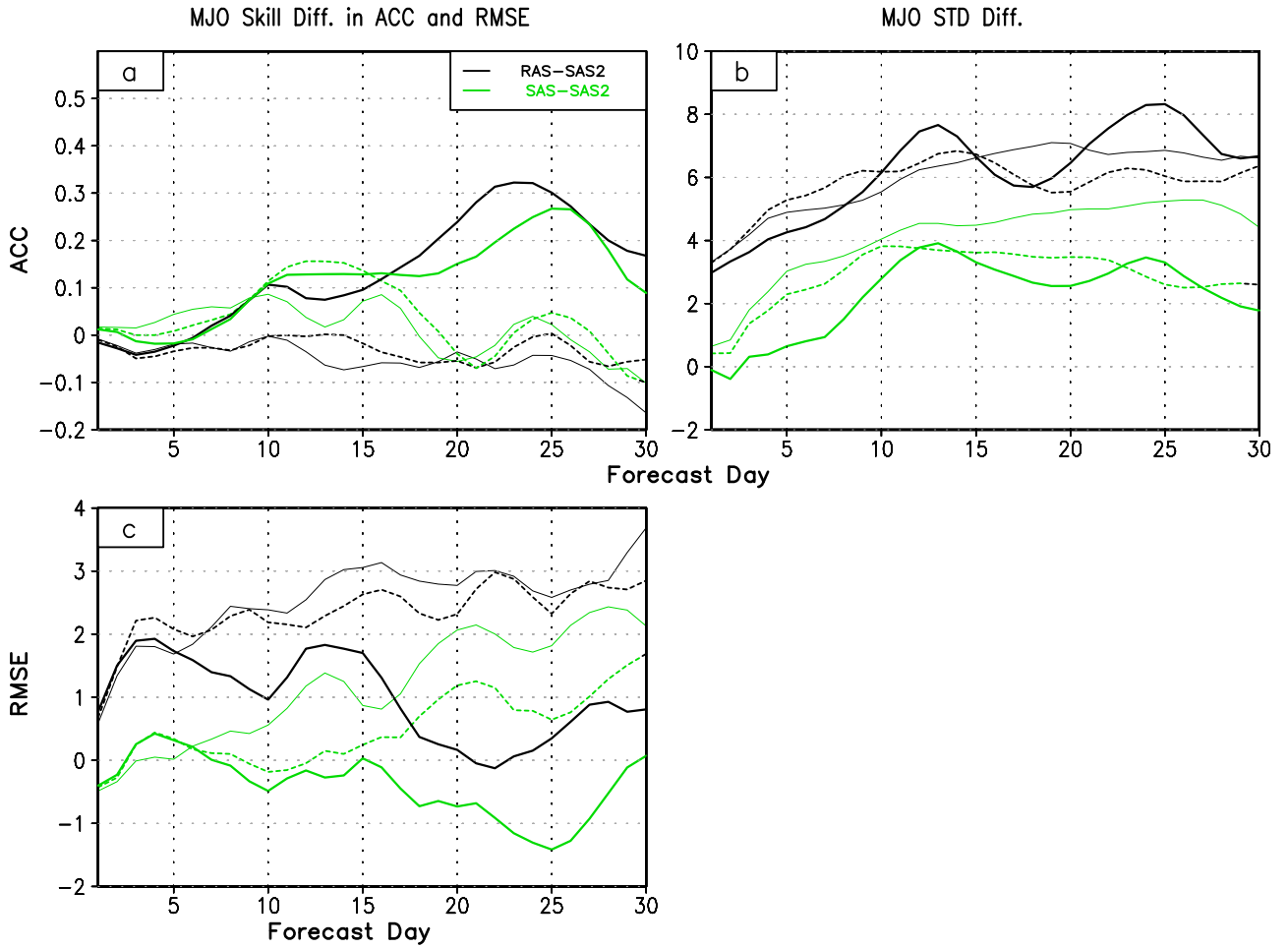


**Figure 7.** Differences of MJO skills measured with the (a) ACC and (c) RMSE and MJO intensity (b) measured with the standard deviation between the (RAS-SAS2) and between the (SAS-SAS2) forced by climatological SST (thin solid lines), NCDC SST (dashed lines), and TMI SST (thick solid lines).

arrival of circum-global upper-level divergence (Zhang et al., 2017) and a dry condition over the Maritime Continent (Figures 10a and 10b). As suggested in previous studies (Wang et al., 2005; Zhao et al., 2013), the dryness centered over the Maritime Continent may help the convection moving into central Indian Ocean (Figures 10c and 10d). The atmospheric internal dynamics are able to sustain the organized convection and propagate it eastward (Figures 10e, 10g, and 10i) with intraseasonal SST anomaly playing a secondary role (Figures 10f, 10h, and 10j). As discussed in section 3, the eastward progression of the Oct-MJO forced by climatological SST is slower than that forced by TMI SST.

For the Nov-MJO (Figure 11), its initiation is likely forced by the positive SST anomaly over the equatorial Indian Ocean and the dryness over the northeastern Indian Ocean instead of the circum-global upper-level forcing (Figures 11c and 11d). Without external intraseasonal SST forcing, the model is unable to sustain the convection over the equatorial western Indian Ocean even with the arrival of circum-global upper-level divergence (Figure 11e). It is very suggestive that the combined effects of the external positive SST anomaly and upper-level divergence sustains the Nov-MJO and leads it to propagate eastward (Figures 11f, 11h, and 11j).

In summary, the Oct-MJO basically reinvigorates over the Indian Ocean in association with the arrival of the circum-global upper-level divergence (Zhang et al., 2017) and the dryness over the Maritime Continent, while an external intraseasonal SST anomaly helps shape the spatial structure and speed up propagation. On the other hand, the Nov-MJO is primarily reinvigorated by a robust positive SST anomaly over the tropical Indian Ocean and the dryness over the northeastern Indian Ocean with the circum-global upper-level divergence playing a very limited role.

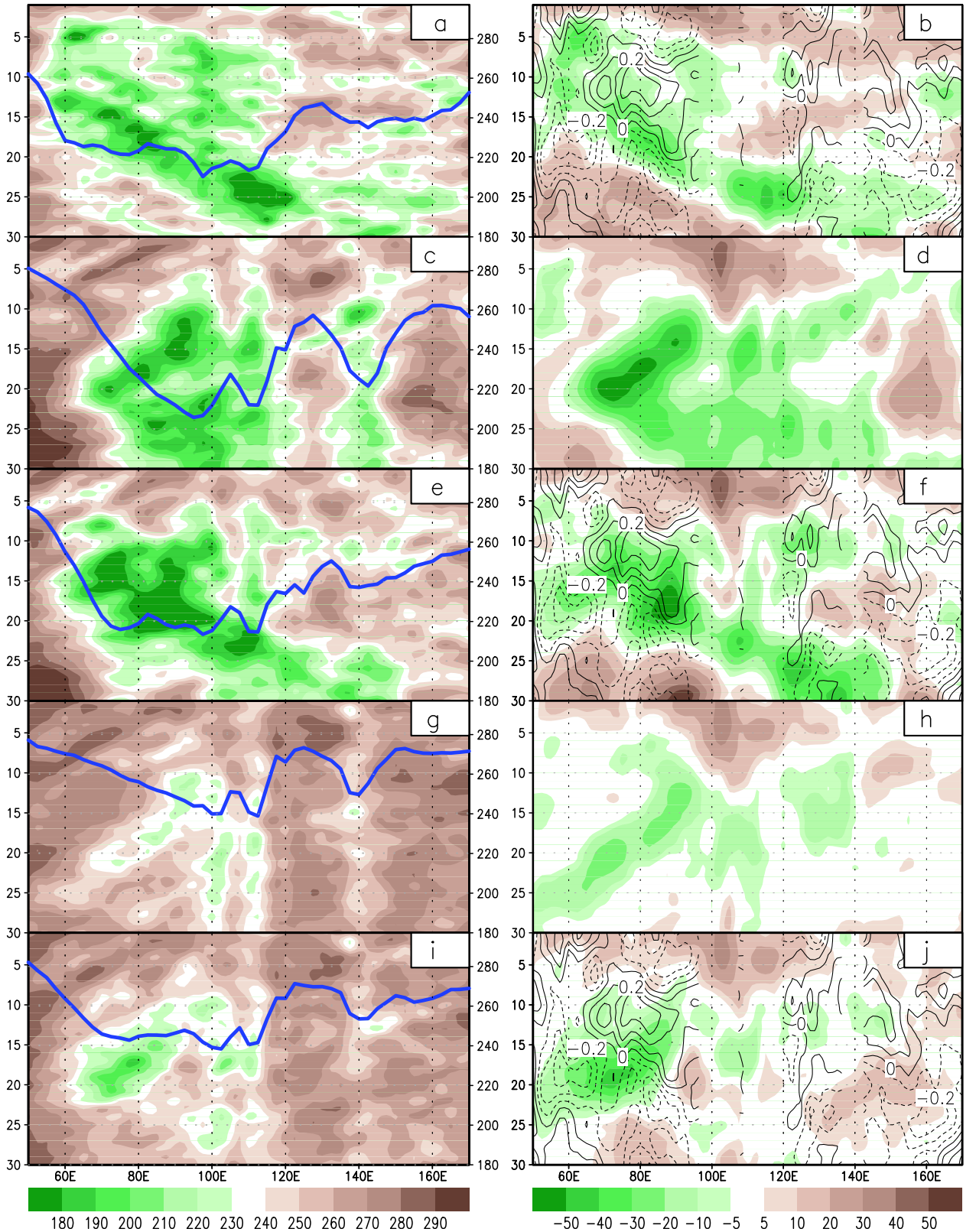


**Figure 8.** Longitude-time evolutions of total OLR (left plots) and OLR (shading, W $m^{-2}$) and SST (contours, CI: 0.1°C) anomalies (right plots) of the Oct-MJO averaged between 10°S and 10°N from (a, b) the observations and the simulations from the RAS with climatological (c, d) SST and (e, f) TMI SST and from the SAS2 with climatological (g, h) SST and (i, j) TMI SST. The thick dark blue lines in left plots represent the monthly mean OLR. The ordinate represents the forecast days starting from 13 October 2011.

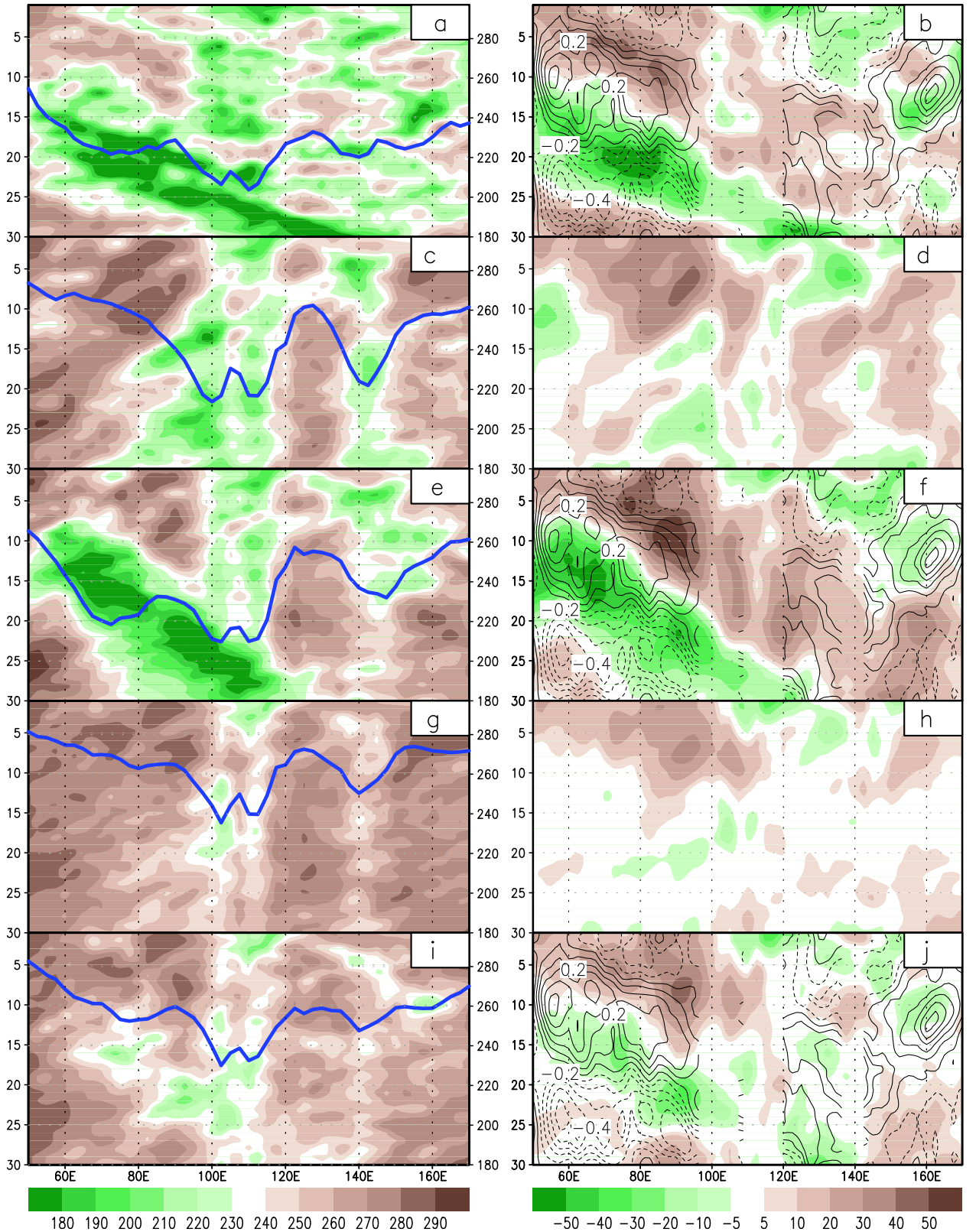


**Figure 9.** Longitude-time evolutions of total OLR (left plots) and OLR (shading, W $m^{-2}$) and SST (contours, CI: 0.1°C) anomalies (right plots) of the Nov-MJO averaged between 10°S and 10°N from (a, b) the observations and the simulations from the RAS with climatological (c, d) SST and (e, f) TMI SST and from the SAS2 with climatological (g, h) SST and (i, j) TMI SST. The thick dark blue lines in left plots represent the monthly mean OLR. The ordinate represents the forecast days starting from 7 November 2011.

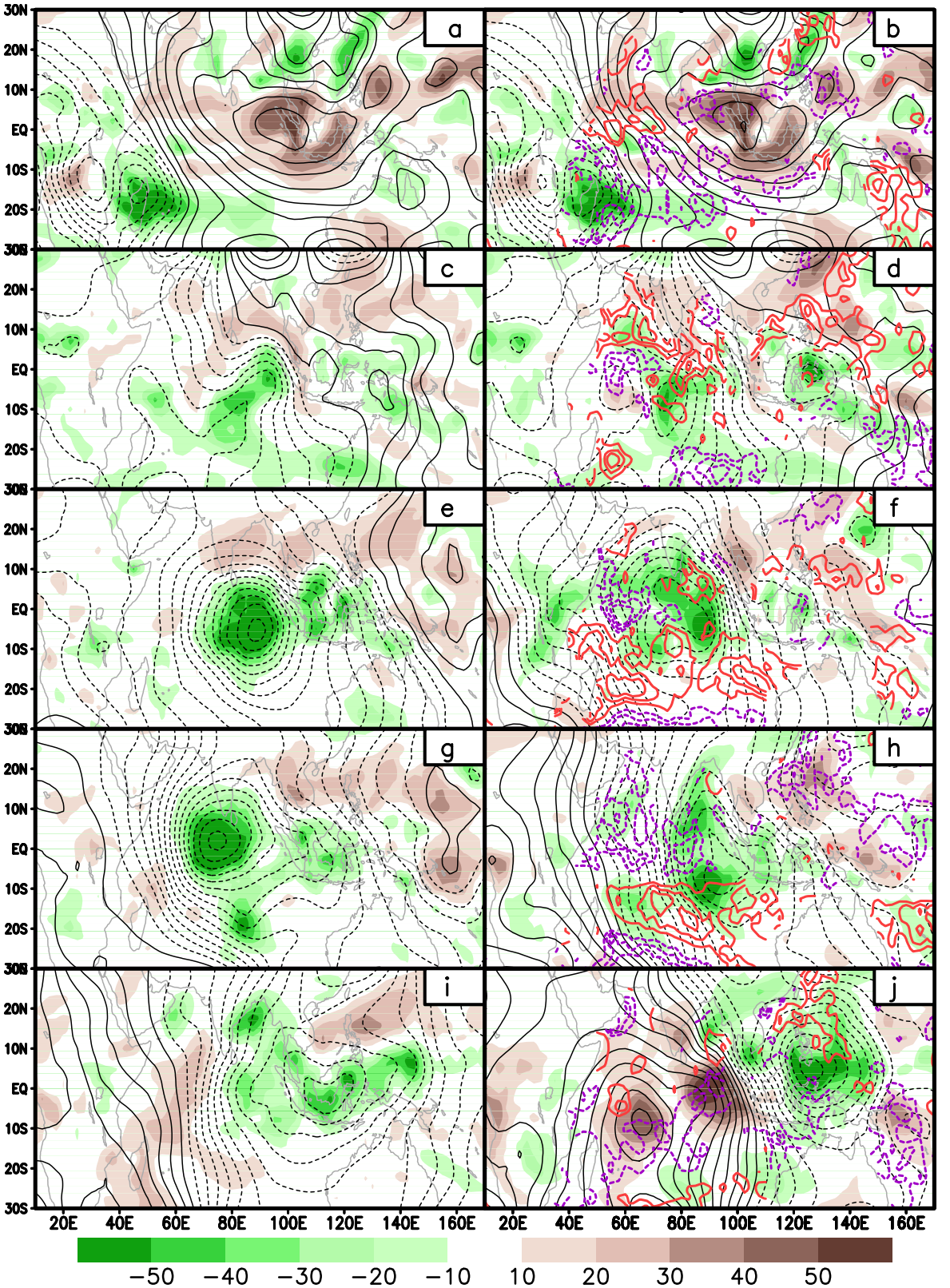


**Figure 10.** Spatiotemporal evolutions of OLR (shading, W $m^{-2}$) and 200 hPa velocity potential anomalies (black contours, CI: $1 \times 10^6$ $m^2$ $s^{-1}$) of the Oct-MJO simulated with the RAS at lead times of days 3, 10, 15, 20, and 30 forced with climatological (a, c, e, g, i) SST and (b, d, f, h, j) TMI SST. The intraseasonal positive (negative) SST anomalies in Figures 10b, 10d, 10f, 10h, and 10j are given in red (purple) with values of 0.2°C, 0.4°C, and 0.6°C (−0.2°C, −0.4°C, and −0.6°C). The initial date is 13 October 2011.

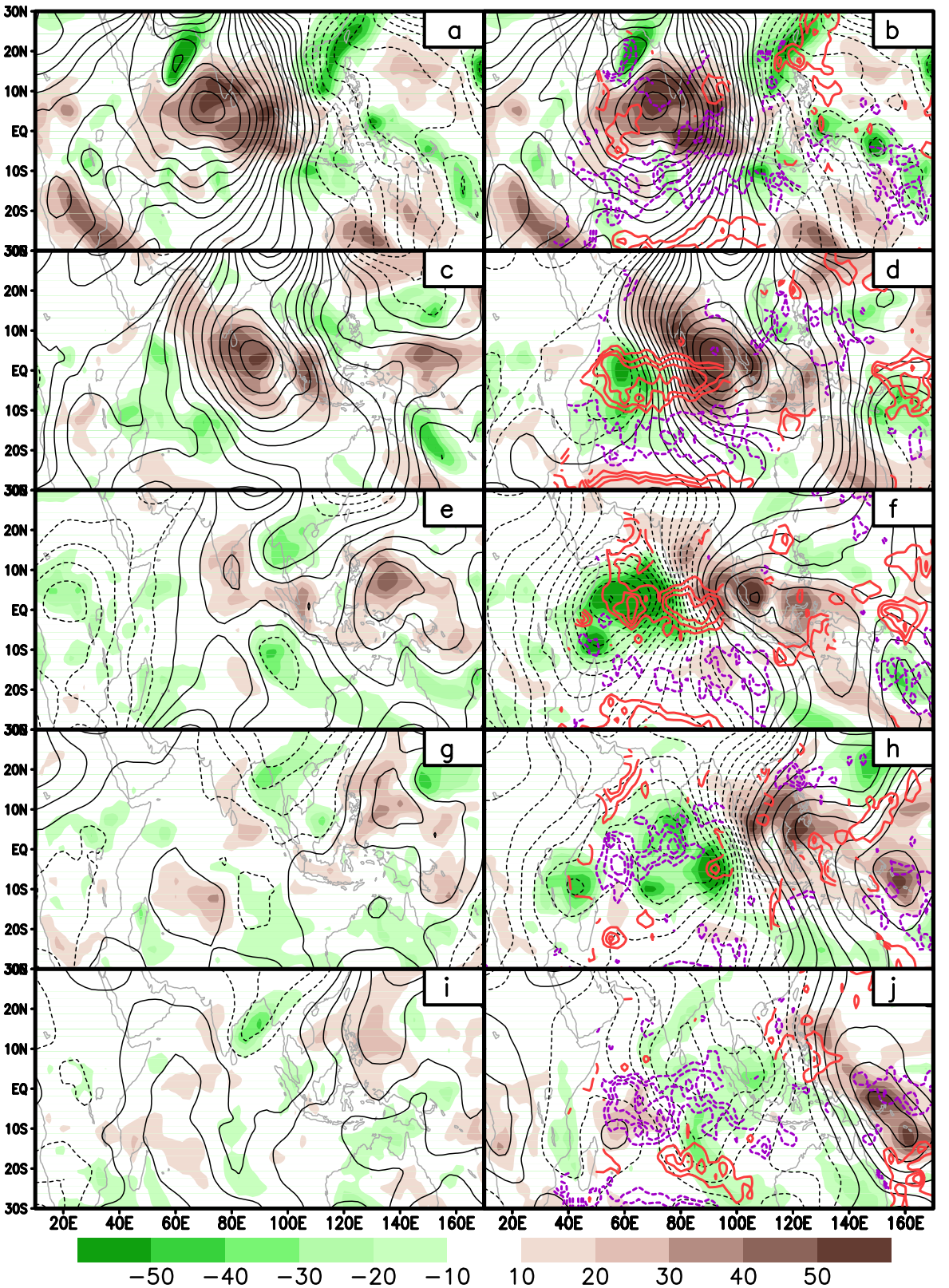


**Figure 11.** Spatiotemporal evolutions of OLR (shading, W $m^{-2}$) and 200 hPa velocity potential anomalies (black contours, CI: $1 \times 10^6$ $m^2$ $s^{-1}$) of the Nov-MJO simulated with the RAS at lead times of days 3, 10, 15, 20, and 30 forced with climatological (a, c, e, g, i) SST and (b, d, f, h, j) TMI SST. The intraseasonal positive (negative) SST anomalies in Figures 11b, 11d, 11f, 11h, and 11j are given in red (purple) with values of 0.2°C, 0.4°C, and 0.6°C (−0.2°C, −0.4°C, and −0.6°C). The initial date is 7 November 2011.

## 5. Discussions and Concluding Remarks

In recent years, air-sea coupled models have become indispensable tools for weather and climate forecasting as well as projecting future climate changes. The common biases on mean states (e.g., double ITCZ) and climate variability (e.g., weak MJO) in these coupled models compromise weather and climate forecasting skills and undermine the confidence of the public on future climate change projections. One of the challenges faced by the community is to reveal the root causes of these biases, which will shed light on ways to improve models and to ensure better forecasts and projections.

This study specifically aims to understand why the impacts of air-sea coupling on MJO simulations are so diverse in present-day global coupled models (e.g., Fu & Wang, 2004; Hendon, 2000; Klingaman & Woolnough, 2014; Newman et al., 2009; Waliser et al., 1999; Watterson & Syktus, 2007; Zhang & Anderson, 2003). As a step toward fully addressing this issue, we analyzed nine sets of hindcasts conducted with NCEP GFS during the DYNAMO period under three different cumulus schemes (RAS, SAS, and SAS2) and three different SST conditions (climatological, NCDC, and TMI). Among the three SST data sets, no intraseasonal anomaly exists in the climatological SST and underestimated and realistic intraseasonal anomalies are present in NCDC SST and TMI SST, respectively (Bhat et al., 2004; Chelton & Wentz, 2005; Harrison & Vecchi, 2001; Maloney et al., 2008; Senguta et al., 2001). Since daily mean NCDC and TMI SSTs are used in this study, the role of diurnal cycle is not investigated here and warrants further research.

Targeting the two MJO events observed during the DYNAMO IOP, we found that without intraseasonal SST forcing, the Oct-MJO can be much better reproduced than the Nov-MJO with all three cumulus schemes. Among them, the RAS (SAS2) maintains strongest (weakest) internal intraseasonal variability with the SAS in the middle (Figure 2). The inclusion of underestimated intraseasonal SST forcing (i.e., NCDC SST) into the hindcasts has little impact on MJO simulations (Figures 1, 5, and 6). Forcing the hindcasts with TMI SST yields significant improvements, in particular for the Nov-MJO, with all three cumulus schemes (Figures 1, 3, 5, and 6). These results suggest that the Oct-MJO is primarily sustained by atmospheric internal dynamics, whereas air-sea coupling is critical for the Nov-MJO. When realistic SST forcing is exerted, the improvement is largest (smallest) with the RAS (SAS2). The resultant MJOs with the RAS agree well with the observations beyond 20 days while the MJOs with the SAS2 become considerably weaker than the observations just after 10 days (Figure 3).

Our results (Figure 4) indicate that the significant response of the MJO to intraseasonally varying SST occurs as early as day 3 from the initial time. Because the MJO exerts significant modulations on global weather and climate systems (Zhang, 2013), coupling the weather and climate forecasting systems to ocean from day 1 would be an ideal strategy (e.g., Janssen et al., 2013) assuming that the initial shock problem can be reasonably overcome (Chen et al., 1997). Although the MJO responds quickly to the intraseasonally varying SST anomaly in the SAS2, the response barely grows as lead time increases, thus resulting in overall weak MJO simulations. On the other hand, the MJO responses to underlying SST anomaly amplify significantly with the RAS and SAS schemes. Therefore, the SST-feedback signals remain very strong with these two schemes even at day 30 (Figure 4).

The impacts of SST-feedbacks on MJO skills among the nine experiments were quantified with the Anomalous Correlation Coefficient (ACC), Root-Mean-Square-Error (RMSE), and intensity that are defined as the standard deviations of intraseasonal OLR anomalies. Without realistic intraseasonal SST forcing (i.e., forced with climatological and NCDC SSTs), the skills measured with the above three indices show mixed results among the three cumulus schemes (Figures 5–7). However, when forcing the hindcasts with TMI SST, the RAS clearly stands out as the best cumulus scheme among the three. This result suggests that the Transpose-AMIP-type simulation forced with realistic SST is a useful approach to evaluate the model capability in representing the MJO and identify the model problems. In addition, we also found that the MJO intensity is likely a better index than the ACC and RMSE as an indicator of model capability in representing the MJO (Figure 7b), in particular when no realistic intraseasonal SST forcing is applied (e.g., forced by climatological and NCDC SSTs). Our finding on the dependence of MJO simulations to a specific cumulus scheme is obtained with the given version of NCEP GFS, further studies with other models are needed to examine in what degree this finding is model dependent.

Detailed analyses were conducted to understand why the Oct-MJO is primarily sustained by atmospheric internal dynamics while the Nov-MJO is strongly coupled to underlying ocean. When initialized on 13

October 2011, all hindcasts using the RAS and SAS2 schemes produced the active phase of the Oct-MJO with and without intraseasonal SST forcing (Figure 8). When initialized on 7 November 2011, only the hindcasts forced with TMI SST captured the Nov-MJO, no matter which cumulus scheme was used (Figure 9). The convection of Oct-MJO is in-phase with the associated positive intraseasonal SST anomaly in both observations (Tseng et al., 2015) and hindcasts (Figure 8) while the associated positive SST anomaly consistently leads the convection of the Nov-MJO by several days. This result suggests that the preconditioning of the Oct-MJO has little to do with external SST forcing and the SST anomaly plays an essential role in preconditioning the onset of the Nov-MJO.

Further analyses reveal that the development of the Oct-MJO is in association with the global circumnavigating mode (Gottschalck et al., 2013; Li et al., 2015; Zhang et al., 2017) and the dryness over the Maritime Continent with the associated intraseasonal SST anomaly playing a secondary role on the propagation speed and spatial structure (Figure 10). On the other hand, the Nov-MJO is primarily reinvigorated by the robust positive SST anomaly over the equatorial Indian Ocean and the dryness over the northeastern Indian Ocean with the circumnavigating mode playing a very limited role (Figure 11).

Our results suggest that the diverse impacts of air-sea coupling on MJO simulations may be attributed to three aspects: (i) diverse effects of air-sea interactions on individual MJO events in the real world (e.g., Moum et al., 2016); (ii) diverse behaviors of various cumulus parameterizations; and (iii) diverse intraseasonal SST anomalies in air-sea coupled models. A too weak internal MJO mode in atmospheric models or a too weak intraseasonal SST anomaly in air-sea coupled models will lead to underestimating the effects of air-sea coupling on MJO simulations. It should be further emphasized that well-represented atmospheric internal MJO mode is a pre-requirement to realistically capture the effects of air-sea coupling on MJO simulations but the inclusion of air-sea coupling would not remedy all biases in atmospheric models. Our present results were obtained using only one model under three variants of Arakawa-Schubert cumulus scheme. Collaborative studies with multimodels are needed to further reveal the causes of diverse impacts of air-sea coupling in present-day coupled models (e.g., CMIP6, Eyring et al., 2016), for example, through comprehensive analysis of the column-integrated moist-static-energy budget (DeMott et al., 2014) and examining the relationships between atmospheric structures of the MJO and its coupling strength with underlying ocean (Chiodi et al., 2014; Li et al., 2014; Moum et al., 2016; Seiki & Takayabu, 2007; Zhang & Anderson, 2003).

Finally, our results indicate that without air-sea interactions there would have been no Nov-MJO, even though it was a successive event following the Oct-MJO. The Oct-MJO, therefore, would have terminated in the Indian Ocean. This result raises the possibility that the existence of some successive MJO events may be rooted in air-sea interactions. This hypothesis is also supported by the observations that a robust intraseasonal SST anomaly is associated with the successive MJO events and propagating MJOs, but not the primary and nonpropagating MJO events (Hirata et al., 2013; Matthews, 2008). An investigation is currently underway to examine this hypothesis.

**Acknowledgments**
This work is supported by NOAA (NA15OAR4310175 and NA16NWS4680019). T. Shinoda is also supported by NSF grants AGS-1347132 and OCE-1658218, NASA grant NNX17AH25G, and NOAA grant NA17OAR4310256. This paper is SOEST contribution number 10264 and IPRC contribution number 1294. The supporting information is being provided online at http://iprc.soest.hawaii.edu/users/xfu/suppl-data/ to enable all the figures in this paper to be reproduced and the full data set is available by contacting me at xfu@hawaii.edu.

## References

Anderson, S. P., Weller, R. A., & Lukas, R. (1996). Surface buoyancy forcing and the mixed layer of the western Pacific warm pool: Observations and 1D model results. *Journal of Climate*, *9*, 3056–3085.

Arakawa, A., & Schubert, W. H. (1974). Interaction of a cumulus ensemble with the large-scale environment, Part I. *Journal of the Atmospheric Sciences*, *31*, 674–704.

Bechtold, P., Koler, M., Jung, T., Doblas-Reyes, F., Leutbecher, M., Rodwell, M. J., . . . Balsamo, G. (2008). Advances in simulating atmospheric variability with the ECMWF model: From synoptic to decadal time-scale. *Quarterly Journal of the Royal Meteorological Society*, *134*, 1337–1351.

Benedict, J. J., & Randall, D. A. (2011). Impacts of idealized air-sea coupling on Madden-Julian Oscillation structure in the superparameterized CAM. *Journal of the Atmospheric Sciences*, *68*, 1990–2008.

Bhat, G. S., Vecchi, G. A., & Gadgil, S. (2004). Sea surface temperature of the Bay of Bengal derived from the TRMM Microwave Imager. *Journal of Atmospheric and Oceanic Technology*, *21*, 1283–1290.

Bjerknes, J. (1969). Atmospheric teleconnections from the equatorial Pacific. *Monthly Weather Review*, *97*, 163–172.

Chelton, D. B., & Wentz, F. J. (2005). Global microwave satellite observations of sea surface temperature for numerical weather prediction and climate research. *Bulletin of the American Meteorological Society*, *86*, 1097–1115.

Chen, D., Zebiak, S. E., & Cane, M. A. (1997). Initialization and predictability of a coupled ENSO forecast model. *Monthly Weather Review*, *125*, 773–788.

Chi, N.-H., Lien, R.-C., D'asaro, E. A., & Ma, B. B. (2014). The surface mixed layer heat budget from mooring observations in the central Indian Ocean during Madden-Julian Oscillation events. *Journal of Geophysical Research: Oceans*, *119*, 4638–4652. https://doi.org/10.1002/2014JC010192

Chiodi, A. M., Harrison, D. E., & Vecchi, G. A. (2014). Subseasonal atmospheric variability and El Nino waveguide warming: Observed effects of the Madden-Julian Oscillation and westerly wind events. *Journal of Climate*, *27*, 3619–3642.
Crueger, T., Stevens, B., & Brokopf, R. (2013). The Madden-Julian Oscillation in ECHAM6 and the introduction of an objective MJO metric. *Journal of Climate*, *26*, 3241–3257.
de Boisseson, E., Balmaseda, M. A., Vitart, F., & Mogensen, K. (2012). Impact of the sea surface temperature forcing on hindcasts of Madden-Julian Oscillation events using the ECMWF model. *Ocean Science*, *8*, 1071–1084.
DeMott, C. A., Klingaman, N. P., & Woolnough, S. J. (2015). Atmosphere-ocean coupled processes in the Madden-Julian Oscillation. *Reviews of Geophysics*, *53*, 1099–1154. https://doi.org/10.1002/2014RG000478
DeMott, C. A., Stan, C., Randall, D. A., & Branson, M. D. (2014). Intra-seasonal variability in coupled GCMs: The roles of ocean feedbacks and model physics. *Journal of Climate*, *27*, 4970–4995.
de Szoeke, S. P., Edson, J. B., Marion, J. R., Fairall, C. W., & Bariteau, L. (2015). The MJO and air-sea interaction in TOGA COARE and DYNAMO. *Journal of Climate*, *28*, 597–622.
Donald, A., Meinke, H., Power, B., Maia, A. de H. N., Wheeler, M. C., White, N., . . . Ribbe, J. (2006). Near-global impact of the Madden-Julian Oscillation on rainfall. *Geophysical Research Letters*, *33*, L09704. https://doi.org/10.1029/2005GL025155
Emanuel, K. A. (1987). An air-sea interaction model of intra-seasonal oscillations in the tropics. *Journal of the Atmospheric Sciences*, *44*, 2324–2340.
Eyring, V., Bony, S., Meehl, G. A., Senior, C. A., Stevens, B., Stouffer, R. J., & Taylor, K. E. (2016). Overview of the Coupled Model Intercomparison Project Phase 6 (CMIP6) experimental design and organization. *Geoscientific Model Development*, *9*, 1937–1958.
Flatau, M., Flatau, P., Phoebus, P., & Niller, P. (1997). The feedback between equatorial convection and local radiative and evaporative processes: The implications for intra-seasonal oscillations. *Journal of the Atmospheric Sciences*, *54*, 2373–2386.
Flatau, M., & Kim, Y.-J. (2013). Interaction between the MJO and polar circulations. *Journal of Climate*, *26*, 3562–3574.
Fu, X., Lee, J.-Y., Hsu, P.-C., Taniguichi, H., Wang, B., Wang, W. Q., & Weaver, S. (2013). Multi-model MJO forecasting during DYNAMO/CINDY period. *Climate Dynamics*, *41*, 1067–1081.
Fu, X., & Wang, B. (2004). Differences of boreal-summer intra-seasonal oscillations simulated in an atmosphere-ocean coupled model and an atmosphere-only model. *Journal of Climate*, *17*, 1263–1271.
Fu, X., Wang, W. Q., Lee, J.-Y., Kikuchi, K., Xu, J. W., Li, J., & Weaver, S. (2015). Distinctive roles of air-sea coupling on different MJO events: A new perspective revealed from the DYNAMO/CINDY field campaign. *Monthly Weather Review*, *143*, 794–812.
Fu, X., Yang, B., Bao, Q., & Wang, B. (2008). Sea surface temperature feedback extends the predictability of tropical intra-seasonal oscillation. *Monthly Weather Review*, *136*, 577–597.
Gottschalck, J., Roundy, P. E., Schreck Iii, C. J., Vintzileos, A., & Zhang, C. D. (2013). Large-scale atmospheric and oceanic conditions during the 2011–12 DYNAMO field campaign. *Monthly Weather Review*, *141*, 4173–4196.
Grabowski, W. W. (2006). Impact of explicit atmosphere-ocean coupling on MJO-like coherent structures in idealized aquaplanet simulations. *Journal of the Atmospheric Sciences*, *63*, 2289–2306.
Green, B. W., Sun, S., Bleck, R., Benjamin, S. G., & Grell, G. A. (2017). Evaluation of MJO predictive skill in multi-physics and multi-model global ensembles. *Monthly Weather Review*, *145*, 2555–2574.
Hamill, T. M., & Kiladis, G. N. (2014). Skill of the MJO and Northern Hemisphere blocking in GEFS medium-range reforecasts. *Monthly Weather Review*, *142*, 868–885.
Han, J., & Pan, H. L. (2011). Revision of convection and vertical diffusion schemes in the NCEP Global Forecast System. *Weather and Forecasting*, *26*, 520–533.
Harrison, D. E., & Vecchi, G. A. (2001). January 1999 Indian Ocean cooling event. *Geophysical Research Letters*, *28*, 3717–3720.
Hendon, H. H. (2000). Impact of air-sea coupling on the Madden-Julian Oscillation in a general circulation model. *Journal of the Atmospheric Sciences*, *57*, 3939–3952.
Higgins, R. W., & Mo, K. C. (1997). Persistent North Pacific circulation anomalies and the tropical intra-seasonal oscillation. *Journal of Climate*, *10*, 223–244.
Hirata, F. E., Webster, P. J., & Toma, V. E. (2013). Distinct manifestations of austral summer tropical intra-seasonal oscillations. *Geophysical Research Letters*, *40*, 3337–3341. https://doi.org/10.1002/grl.50632
Hirst, A. C., & Lau, K.-M. (1990). Intra-seasonal and interannual oscillations in coupled ocean-atmosphere models. *Journal of Climate*, *3*, 713–725.
Hoyos, C. D., & Webster, P. J. (2007). The role of intra-seasonal variability in the nature of Asian monsoon precipitation. *Journal of Climate*, *20*, 4402–4424.
Inness, P. M., Slingo, J. M., Guilyardi, E., & Cole, J. (2003). Simulation of the Madden-Julian Oscillation in a coupled general circulation model. Part II: The role of the basic state. *Journal of Climate*, *16*, 365–382.
Janssen, P., Breivik, O., Mogensen, K., Vitart, F., Balmaseda, M., Bidlot, J.-R., . . . Molteni, F. (2013). *Air-sea interaction and surface waves* (ECMWF Tech. Mem. 712). Retrieved from https://www.ecmwf.int/en/elibrary/10238-air-sea-interaction-and-surface-waves
Kawamura, R. (1988). Intra-seasonal variability of sea surface temperature over the tropical western Pacific. *Journal of the Meteorological Society of Japan*, *66*, 1007–1012.
Kemball-Cook, S., Wang, B., & Fu, X. (2002). Simulation of the intra-seasonal oscillation in the ECHAM4 model: The impact of coupling with an ocean model. *Journal of the Atmospheric Sciences*, *59*, 1433–1453.
Klingaman, N. P., & Woolnough, S. J. (2014). The role of air-sea coupling in the simulation of the Madden-Julian Oscillation in the Hadley Centre model. *Quarterly Journal of the Royal Meteorological Society*, *140*, 2272–2286.
Knutson, T. R., & Weickmann, K. M. (1987). 30–60 day atmospheric oscillations: Composite life cycles of convection and circulation anomalies. *Monthly Weather Review*, *115*, 1407–1436.
Krishnamurti, T. N., Jayakumar, P. K., Sheng, J., Surgi, N., & Kumar, A. (1985). Divergent circulations on the 30 to 50-day time scale. *Journal of the Atmospheric Sciences*, *42*, 364–375.
Krishnamurti, T. N., Oosterhof, D. K., & Metha, A. V. (1988). Air-sea interaction on the timescale of 30–50 days. *Journal of the Atmospheric Sciences*, *45*, 1304–1322.
Lau, K.-M., & Shen, S. (1988). On the dynamics of intra-seasonal oscillations and ENSO. *Journal of the Atmospheric Sciences*, *45*, 1781–1797.
Li, C. Y., & Liao, Q. H. (1996). Behavior of coupled modes in a simple nonlinear air-sea interaction model. *Advances in Atmospheric Sciences*, *13*, 183–195.
Li, T., Zhao, C. B., Hsu, P.-C., & Nasuno, T. (2015). MJO initiation processes over the tropical Indian Ocean during DYNAMO/CINDY2011. *Journal of Climate*, *28*, 2121–2135.
Li, Y., Han, W., Shinoda, T., Wang, C., Ravichandran, M., & Wang, J.-W. (2014). Revisiting the wintertime intraseasonal SST variability in the tropical south Indian Ocean: Impact of the ocean interannual variation. *Journal of Physical Oceanography*, *44*, 1886–1907.

Liess, S., Bengtsson, L., & Arpe, K. (2004). The intra-seasonal oscillation in ECHAM4. Part I: Coupled to a comprehensive ocean model. *Climate Dynamics*, *22*, 671–688.
Lin, H., Brunet, G., & Derome, J. (2009). An observed connection between the North Atlantic Oscillation and the Madden-Julian Oscillation. *Journal of Climate*, *22*, 364–380.
Liu, F., & Wang, B. (2013). An air-sea coupled skeleton model for the Madden-Julian Oscillation. *Journal of the Atmospheric Sciences*, *70*, 3147–3156.
Lorenc, A. C. (1984). The evolution of planetary-scale 200-mb divergent flow during the FGGE year. *Quarterly Journal of the Royal Meteorological Society*, *110*, 427–441.
Madden, R. A., & Julian, P. R. (1971). Detection of a 40–50-day oscillation in zonal wind in the tropical Pacific. *Journal of the Atmospheric Sciences*, *28*, 702–708.
Madden, R. A., & Julian, P. R. (1972). Description of global-scale circulation cells in tropics with a 40–50-day period. *Journal of the Atmospheric Sciences*, *29*, 1109–1123.
Maloney, E. D., Chelton, D. B., & Esbensen, S. K. (2008). Subseasonal SST variability in the tropical eastern north Pacific during boreal summer. *Journal of Climate*, *21*, 4149–4167.
Maloney, E. D., & Hartmann, D. L. (2001). The sensitivity of intra-seasonal variability in the NCAR CCM3 to changes in convective parameterization. *Journal of Climate*, *14*, 2015–2034.
Marshall, A. G., Alves, O., & Hendon, H. H. (2008). An enhanced moisture convergence-evaporation feedback mechanism for MJO air-sea interaction. *Journal of the Atmospheric Sciences*, *65*, 970–986.
Matsueda, M., & Endo, H. (2011). Verification of medium-range MJO forecasts with TIGGE. *Geophysical Research Letters*, *38*, L11801. https://doi.org/10.1029/2011GL047480
Matthews, A. J. (2008). Primary and successive events in the Madden-Julian Oscillation. *Quarterly Journal of the Royal Meteorological Society*, *134*, 439–453.
Miura, H., Satoh, M., Nasuno, T., Noda, A. T., & Oouchi, K. (2007). A Madden-Julian Oscillation event realistically simulated by a global cloud-resolving model. *Science*, *318*, 1763–1765. https://doi.org/10.1126/science.1148443
Moorthi, S., & Suarez, M. J. (1992). Relaxed Arakawa-Schubert: A parameterization of moist convection for general circulation model. *Monthly Weather Review*, *120*, 978–1002.
Moorthi, S., & Suarez, M. J. (1999). *Documentation of version 2 of relaxed Arakawa-Schubert cumulus parameterization with convective downdrafts* (NOAA Office Note 99-01, 44 pp.). Camp Springs, MD: National Centers for Environmental Prediction.
Moum, J. N., de Szoeke, S. P., Smyth, W. D., Edson, J. B., DeWitt, H. L., Moulin, A. J., . . . Fairall, C. W. (2014). Air-sea interactions from westerly wind bursts during the November 2011 MJO in the Indian Ocean. *Bulletin of the American Meteorological Society*, *95*, 1185–1199.
Moum, J. N., Pujiana, K., Lien, R.-C., & Smyth, W. D. (2016). Ocean feedback to pulses of the Madden-Julian Oscillation in the equatorial Indian Ocean. *Nature Communications*, *7*, 13203. https://doi.org/10.1038/ncomms13203
Neelin, J. D., Held, I. M., & Cook, K. H. (1987). Evaporation-wind feedback and low-frequency variability in the tropical atmosphere. *Journal of the Atmospheric Sciences*, *44*, 2341–2348.
Newman, M., Sardeshmukh, P. D., & Penland, C. (2009). How important is air-sea coupling in ENSO and MJO evolution. *Journal of Climate*, *22*, 2958–2977.
Pan, H.-L., & Wu, W.-S. (1995). *Implementing a mass flux convection parameterization package for the NMC medium-range forecast model* (NMC Office Note 409, 39 pp.). Washington, DC: National Oceanic and Atmospheric Administration.
Pegion, K., & Kirtman, B. P. (2008). The impact of air-sea interactions on the predictability of the tropical intraseasonal oscillation. *Journal of Climate*, *21*, 5870–5886.
Phillips, T. J., Potter, G. L., Williamson, D. L., Cederwall, R. T., Boyle, J. S., Fiorino, M., . . . Yio, J. J. (2004). Evaluating parameterizations in general circulation models: Climate simulation meets weather prediction. *Bulletin of the American Meteorological Society*, *85*, 1903–1915.
Reynolds, R. W., & Smith, T. M. (1994). Improved global sea surface temperature analyses using optimum interpolation. *Journal of Climate*, *7*, 929–948.
Saha, S., Moorthi, S., Pan, H.-L., Wu, X., Wang, J., Nadiga, S., . . . Goldberg, M. (2010). The NCEP Climate Forecast System reanalysis. *Bulletin of the American Meteorological Society*, *91*, 1015–1057.
Saha, S., Moorthi, S., Wu, X., Wang, J., Nadiga, S., Tripp. P, . . . Becker, E. (2014). The NCEP Climate Forecast System version 2. *Journal of Climate*, *27*, 2185–2208.
Seiki, A., & Takayabu, Y. N. (2007). Westerly wind bursts and their relationship and intraseasonal variations and ENSO. Part I: Statistics. *Monthly Weather Review*, *135*, 3325–3345.
Senguta, D., Goswami, B. N., & Senan, R. (2001). Coherent intraseasonal oscillations of ocean and atmosphere during the Asian summer monsoon. *Geophysical Research Letters*, *28*, 4127–4130.
Shinoda, T., Hendon, H. H., & Glick, J. (1998). Intra-seasonal variability of surface fluxes and sea surface temperature in the tropical western Pacific and Indian oceans. *Journal of Climate*, *11*, 1685–1702.
Sobel, A. H., & Gildor, H. (2003). A simple time-dependent model for SST hot spots. *Journal of Climate*, *16*, 3978–3992.
Sperber, K. R., Gualdi, S., Legutke, S., & Gayler, V. (2005). The Madden-Julian Oscillation in ECHAM4 coupled and uncoupled GCMs. *Climate Dynamics*, *25*, 117–140.
Tseng, K.-C., Sui, C.-H., & Li, T. (2015). Moistening processes for Madden-Julian Oscillations during DYNAMO/CINDY. *Journal of Climate*, *28*, 3041–3057.
Waliser, D. E., Lau, K. M., & Kim, J. H. (1999). The influence of coupled sea-surface temperatures on the Madden-Julian Oscillation: A model perturbation experiment. *Journal of the Atmospheric Sciences*, *56*, 333–358.
Wang, B., & Li, T. (1994). Convective interaction with boundary-layer dynamics in the development of the tropical intra-seasonal system. *Journal of the Atmospheric Sciences*, *51*, 1386–1400.
Wang, B., Webster, P. J., & Teng, H. (2005). Antecedents and self-induction of active-break south Asian monsoon unraveled by satellites. *Geophysical Research Letters*, *32*, L04704. https://doi.org/10.1029/2004GL020996
Wang, B., & Xie, X. (1998). Coupled modes of the warm pool climate system. Part I: The role of air-sea interaction in maintaining Madden-Julian Oscillation. *Journal of Climate*, *11*, 2116–2135.
Wang, S. G., Sobel, A. H., Zhang, F. Q., Sun, Y. Q., Yue, Y., & Zhou, L. (2015). Regional simulation of the October and November MJO events observed during the CINDY/DYNAMO field campaign at gray zone resolution. *Journal of Climate*, *28*, 2097–2119.
Wang, W. Q., Kumar, A., Fu, J. X., & Huang, H.-P. (2015). Dependence of MJO prediction on sea surface temperatures and convection schemes. *Monthly Weather Review*, *143*, 3156–3174.

Watterson, I. G., & Syktus, J. (2007). The influence of air-sea interaction on the Madden-Julian Oscillation: The role of the seasonal mean state. *Climate Dynamics*, *28*, 703–722.

Wentz, F. J., Gentemann, C. L., Smith, D. K., & Chelton, D. B. (2000). Satellite measurements of sea surface temperature through clouds. *Science*, *288*, 847–850. https://doi.org/10.1126/science

Yoneyama, K., Zhang, C., & Long, C. N. (2013). Tracking the pulses of the Madden-Julian Oscillation. *Bulletin of the American Meteorological Society*, *94*, 1871–1891.

Zhang, C. D. (2013). Madden-Julian Oscillation: Bridging weather and climate. *Bulletin of the American Meteorological Society*, *94*, 1849–1870.

Zhang, C. D., & Anderson, S. P. (2003). Sensitivity of intra-seasonal perturbations in SST to the structure of the MJO. *Journal of the Atmospheric Sciences*, *60*, 2196–2207.

Zhang, F. Q., Taraphdar, S., & Wang, S. (2017). The role of global circumnavigating mode in the MJO initiation and propagation. *Journal of Geophysical Research: Atmospheres*, *122*, 5837–5856. https://doi.org/10.1002/2016JD025665

Zhao, C., Li, T., & Zhou, T. (2013). Precursor signals and processes associated with MJO initiation over the tropical Indian Ocean. *Journal of Climate*, *26*, 291–307.